30 December 1994

ELSEVIER

Chemical Physics Letters 231 (1994) 373-379

CHEMICAL PHYSICS LETTERS

Exciton confinement effects in nonlinear optical spectroscopy of interacting quantum wires

Ningjun Wang [1], Shaul Mukamel

Department of Chemistry, University of Rochester, Rochester, NY 14627, USA

Received 16 August 1994; in final form 13 October 1994

Abstract

Nonlinear light scattering and four-wave mixing from N interacting quantum wires are calculated using Green function techniques. Size confinement results in discrete single- and two-photon resonances. The nonlinear signal per wire increases with N for small N, and saturates at large N. Effects of interactions within wires and among wires on the nonlinear signal and the coherence size are analyzed. The shapes of single-photon resonances for small N (quasi 1D) and for large N (quasi 2D) are compared.

Nonlinear optical response of molecular assemblies such as dye aggregates, crystals, and artificial structures such as organic superlattices [1-3] is usually interpreted using the Frenkel or the charge-transfer exciton model [4,5]; a few reports have even suggested that excitons in anthracence crystal are of the Wannier type [6,7]. Exciton eigenstates in geometrically restricted systems have a discrete spectrum, and the oscillator strength is not evenly distributed among the eigenstates [8-11]. Some states carry a large oscillator strength that is proportional to the system size, and show cooperative spontaneous emission [12-14] and size enhancement of the nonlinear optical response [11,15,16]. The conventional procedure for calculating the four-wave mixing (FWM) signal consists of two steps: first one calculates the third-order nonlinear susceptibility $\chi^{(3)}$ by solving the single- and the two-exciton eigenstates, and then the Maxwell equation is solved using the calculated $\chi^{(3)}$. Both steps are not straightforward for a molecular assembly with complex geometry. A nonlocal variation of the procedure was used by Ishihara and Cho to study the size dependence of the third order nonlinear optical response of molecular multilayers [17].

Chernyak and Mukamel derived a Green function expression (GFE) for the third-order nonlinear optical response functions of molecular assemblies with arbitrary geometry [18]. It incorporates the nonlocal properties of both $\chi^{(3)}$ and the internal field, and expresses the signal explicitly in terms of the single particle Green functions that are related only to single exciton eigenstates. The GFE shows the existence of a coherence size which controls the magnitude of the cooperative nonlinear response [19].

In this Letter, we apply the GFE to study the size scaling of the nonlinear light scattering and FWM of interacting chains of two-level molecules which form Frenkel excitons. The coherence size N_c, defined as the number of wires that maximizes the nonlinear signal per wire, is calculated. The nonlinear light

[1] Present address: Department of Chemistry, Princeton University, Princeton, NJ 08544, USA.

SSDI 0009-2614(94)01291-1

scattering spectrum shows distinct two-photon resonances reflecting size confinement in the interwire direction. The magnitude of the two-photon resonance and the coherence size are both affected by the Coulomb interactions among molecules. The roles of intrawire and interwire interactions are examined separately. By varying the number of wires, we demonstrate how the spectra reflect the evolution of 1D to 2D excitons.

Consider a nanostructure made of N molecular wires of length M forming a two-dimensional $M\times N$ molecular lattice with lattice vectors $a\hat{x}$ and $a\hat{y}$, a being the lattice constant. Each molecule has two electronic levels with energy gap Ω and transition dipole moment $\boldsymbol{\mu}$, but no permanent dipole moment. The Hamiltonian is

$$H=\Omega\sum_{n\lambda}B_{n\lambda}^{+}B_{n\lambda}+\sum_{n\lambda,m\mu}J_{n\lambda,m\mu}B_{n\lambda}^{+}B_{m\mu}-\sum_{n\lambda}\hat{\boldsymbol{P}}_{n\lambda}\cdot\boldsymbol{E}(\boldsymbol{r}_{n\lambda},t)\,, \tag{1}$$

where $\lambda,\mu=1,\ldots,N$ denote position in the y direction and $m,n=1,\ldots,M$ denote the position along the x direction. N is small and we shall set M to infinity at the end of the calculation. The molecular positions are $\boldsymbol{r}_{n\lambda}=na\hat{\boldsymbol{x}}+\lambda a\hat{\boldsymbol{y}}$. B^{+} and B are exciton creation and annihilation operators with commutation rules

$$[B_{n\lambda},B_{m\mu}^{+}]=\delta_{nm}\delta_{\lambda\mu}(1-2B_{n\lambda}^{+}B_{n\lambda})\,. \tag{2}$$

The nearest neighbor coupling $J_{n\lambda,m\mu}$ has the form

$$J_{n\lambda,m\mu}=-J(\delta_{n,m+1}+\delta_{n,m-1})\delta_{\lambda,\mu}-J'(\delta_{\lambda,\mu+1}+\delta_{\lambda,\mu-1})\delta_{nm}\,, \tag{3}$$

where $-J$ and $-J'$ are dipole–dipole coupling matrix elements along the x (intrawire) and y (interwire) directions, respectively. The last term in Eq. (1) represents the interaction with a classical electromagnetic field $\boldsymbol{E}$, and the polarization operator of the nth molecules at the λth chain is

$$\hat{\boldsymbol{P}}_{n\lambda}=\boldsymbol{\mu}(B_{n\lambda}+B_{n\lambda}^{+})\,. \tag{4}$$

In a nonlinear light scattering experiment the system interacts with an external monochromatic electric field

$$\boldsymbol{E}(\boldsymbol{r},t)=\boldsymbol{E}\exp(\mathrm{i}\boldsymbol{k}\cdot\boldsymbol{r}-\mathrm{i}\omega t)+\text{c.c.}\,, \tag{5}$$

where c.c. denotes the complex conjugate. The scattered field $E_{\mathrm{sc}}(\boldsymbol{R},\omega)$ is detected at position $\boldsymbol{R}$ far from the lattice with $k'_x=k_x$, where $\boldsymbol{k}'\equiv\omega\boldsymbol{R}/Rc$ is the outgoing wavevector. The scattered signal expanded in powers of the incident field is

$$I(\omega)=|E_{\mathrm{sc}}(\boldsymbol{R},\omega)|^2=N^2[S_{\mathrm{LR}}(\omega)|E|^2+S_{\mathrm{NR}}(\omega)|E|^4+\mathcal{O}(|E|^6)]\,, \tag{6}$$

where S_{LR} and S_{NR} are the linear and lowest-order nonlinear scattering coefficients per wire,

$$S_{\mathrm{LR}}(\omega)=|E_{\mathrm{sc}}^{(1)}(\boldsymbol{R},\omega)|^2/|E|^2N^2\,, \tag{7}$$

$$S_{\mathrm{NR}}(\omega)=2\,\mathrm{Re}[E_{\mathrm{sc}}^{(1)*}(\boldsymbol{R},\omega)E_{\mathrm{sc}}^{(3)}(\boldsymbol{R},\omega)]/|E|^4N^2\,. \tag{8}$$

Here the superscripts denote the order with respect to the incident field. For noninteracting wires ($J'=0$), each wire scatters the field independently, E_{sc} is proportional to N, and S_{LR} and S_{NR} are independent of N.

Both $E_{\mathrm{sc}}^{(1)}$ and $E_{\mathrm{sc}}^{(3)}$ contribute to the nonlinear scattering. $E_{\mathrm{sc}}^{(3)}$ can be observed directly by a FWM measurement with heterodyne detection, where four waves with the same frequency ω are incident on the system

$$\boldsymbol{E}(\boldsymbol{r},t)=\sum_{i=1}^{4}\boldsymbol{E}_i\exp(\mathrm{i}\boldsymbol{k}_i\cdot\boldsymbol{r}-\mathrm{i}\omega t)+\text{c.c.} \tag{9}$$

The first three waves generate the signal. The fourth wave with wavevector $k_{4x}=k_{1x}-k_{2x}+k_{3x}$ is in the direction of the signal and serves as a local oscillator. The signal field with wavevector $\boldsymbol{k}_4$ to lowest order in the external field is

$$\boldsymbol{E}_{\mathrm{sc}}(\boldsymbol{R},\omega_{\mathrm{s}})=[N\boldsymbol{\gamma}^{(3)}(-\omega;\omega,-\omega,\omega)\cdot\boldsymbol{E}_1\boldsymbol{E}_2^{*}\boldsymbol{E}_3+\boldsymbol{E}_4]\times\exp(\mathrm{i}\omega R/c)\,, \tag{10}$$

and the signal is given by

$$S_{\mathrm{FWM}}(\omega_{\mathrm{s}})=2N\,\mathrm{Re}(\boldsymbol{\gamma}^{(3)}\cdot\boldsymbol{E}_1\boldsymbol{E}_2^{*}\boldsymbol{E}_3\boldsymbol{E}_4^{*})\,, \tag{11}$$

where $\boldsymbol{\gamma}^{(3)}$ is a fourth-rank tensor and will be specified below. Assuming that $\boldsymbol{E}_1$ and $\boldsymbol{E}_2$ have the same phase, then by controlling the relative phase of $\boldsymbol{E}_3$ and $\boldsymbol{E}_4$, one can measure the real and imaginary parts of $\boldsymbol{\gamma}^{(3)}$. If they are in phase then the signal is proportional to $\mathrm{Re}\,\gamma^{(3)}$, whereas if the phase differed by $\pi/2$ we get $\mathrm{Im}\,\gamma^{(3)}$.

We first consider the light scattering experiment. Following the Green function procedure of Refs.

[11,19], we obtain the linear and third-order nonlinear polarization in the rotating wave approximation (RWA),

$$\boldsymbol{P}_{n\lambda}(t)=\langle\hat{\boldsymbol{P}}_{n\lambda}\rangle=\boldsymbol{P}_{\lambda}(k_x)\exp(\mathrm{i}k_x na-\mathrm{i}\omega t)\,, \quad (12a)$$

$$\boldsymbol{P}^{(1)}_{\lambda}(k_x)=-\boldsymbol{\mu}(\boldsymbol{\mu}\cdot\boldsymbol{E})\sum_{\mu}G_{\lambda\mu}(k_x,\omega)\exp(\mathrm{i}k_y\mu a)\,, \quad (12b)$$

$$\boldsymbol{P}^{(3)}_{\lambda}(k_x)=-\tfrac{1}{2}(\boldsymbol{\mu}\cdot\boldsymbol{E})^2(\boldsymbol{\mu}\cdot\boldsymbol{E})^*\boldsymbol{\mu}\sum_{\lambda'\lambda''\mu_3\mu_2\mu_1}G_{\lambda\lambda'}(k_x,\omega)$$
$$\times G^*_{\lambda'\mu_3}(k_x,\omega)G_{\lambda''\mu_2}(k_x,\omega)G_{\lambda''\mu_1}(k_x,\omega)$$
$$\times\bar{\Gamma}_{\lambda'\lambda''}(2k_x,2\omega)\exp[\mathrm{i}k_y(\mu_1+\mu_2-\mu_3)a]\,, \quad (12c)$$

where $P^{(1)}$ and $P^{(3)}$ denote the linear and the third-order polarization (the second-order polarization vanishes since we assume that the molecules have no permanent dipole moment).

The single-particle Green function G is

$$G_{\lambda\mu}(k_x,\omega)=[\omega+\mathrm{i}\eta-\Omega-J(k_x)]^{-1}_{\lambda\mu}\,, \quad (13)$$

where η is a nonradiative excitation decay rate which is assumed to be much larger than the radiative decay rate. $J(k_x)$ is an N by N matrix with elements

$$J_{\lambda\mu}(k_x)=\sum_{m\neq n}J_{n\lambda,m\mu}\exp[-\mathrm{i}k_x(n-m)a]$$
$$=-2J\cos(k_xa)\delta_{\lambda\mu}-J'(\delta_{\lambda,\mu+1}+\delta_{\lambda,\mu-1})\,. \quad (14)$$

The scattering matrix $\bar{\Gamma}$ in Eq. (12c) is given by

$$\bar{\Gamma}_{\lambda\mu}(2k_x,2\omega)=-2[F(2k_x,2\omega)]^{-1}_{\lambda\mu}\,, \quad (15a)$$

$$F_{\lambda\mu}(2k_x,2\omega)=\frac{\mathrm{i}a}{4\pi^2}\int\mathrm{d}k'_x\,\mathrm{d}\omega'\,G_{\lambda\mu}(k'_x,\omega')$$
$$\times G_{\lambda\mu}(2k_x-k'_x,2\omega-\omega')\,. \quad (15b)$$

When the $J_{\lambda\mu}(k_x)$ matrix (Eq. (14)) is diagonalized, we find that the energy and wavefunction of the αth single-exciton eigenstate with momentum k_x along x is

$$\epsilon_{\alpha}(k_x)=\Omega-2J\cos(k_xa)-2J'\cos[\alpha\pi/(N+1)]\,,$$
$$\alpha=1,2,\ldots,N\,, \quad (16)$$

$$\psi_{\alpha k_x}(\lambda,n)=\frac{1}{\sqrt{M}}\psi_{\alpha}(\lambda)\exp(\mathrm{i}k_xna)\,, \quad (17)$$

with

$$\psi_{\alpha}(\lambda)=\sqrt{\frac{2}{N+1}}\sin[\lambda\alpha\pi/(N+1)]\,. \quad (18)$$

Here $\epsilon_{\alpha}(k_x)$ and $\psi_{\alpha}(\lambda)$ are the eigenvalues and eigenvectors of $J_{\lambda\mu}(k_x)$. Note that for nearest neighbor interaction $\psi_{\alpha}(\lambda)$ does not depend on k_x. Using these eigenvectors we obtain

$$G_{\lambda\mu}(k_x,\omega)=\sum_{\alpha}\frac{\psi_{\alpha}(\lambda)\psi^*_{\alpha}(\mu)}{\omega-\epsilon_{\alpha}(k_x)+\mathrm{i}\eta}\,, \quad (19)$$

$$F_{\lambda\mu}(0,2\omega)=\frac{a}{2\pi}$$
$$\times\int\mathrm{d}k'_x\sum_{\alpha\beta}\frac{\psi_{\alpha}(\lambda)\psi^*_{\alpha}(\mu)\psi_{\beta}(\lambda)\psi^*_{\beta}(\mu)}{2\omega-\epsilon_{\alpha}(k'_x)-\epsilon_{\beta}(-k'_x)+2\mathrm{i}\eta}$$
$$=\tfrac{1}{2}\sum_{\alpha\beta}\psi_{\alpha}(\lambda)\psi^*_{\alpha}(\mu)\psi_{\beta}(\lambda)\psi^*_{\beta}(\mu)$$
$$\times(\{\omega-\Omega+\mathrm{i}\eta+J'\cos[\alpha\pi/(N+1)]$$
$$+J'\cos[\beta\pi/(N+1)]\}^2-(2J)^2)^{-1/2}\,. \quad (20)$$

Here the k'_x integration has been performed analytically using the method of Section 5.3.1 of Ref. [20]. The scattered field at position $\boldsymbol{R}$ in the far zone is [19]

$$\boldsymbol{E}_{\mathrm{sc}}(\boldsymbol{R},\omega)\propto M\frac{\Omega^2}{RC^2}$$
$$\times\exp(\mathrm{i}\omega R/c)\sum_{\lambda}(\mathbf{1}-\hat{\boldsymbol{R}}\hat{\boldsymbol{R}})\cdot\boldsymbol{P}_{\lambda}(k_x)$$
$$\times\exp(-\mathrm{i}k'_y\lambda a)\delta_{k'_x,k_x}\,, \quad (21)$$

where $\boldsymbol{k}'=\omega\hat{\boldsymbol{R}}/c$ is the signal wavevector, and $\hat{\boldsymbol{R}}=\boldsymbol{R}/R$. Substituting Eqs. (12) and (21) into Eqs. (7) and (8), we finally obtain

$$S_{\mathrm{LR}}(\omega)=|E^{(1)}_{\mathrm{sc}}(\boldsymbol{R},\omega)|^2/E^2N^2$$
$$\propto\left|\sum_{\lambda}G_{\lambda}(\omega)\right|^2\Big/N^2\,, \quad (22)$$

$$S_{\mathrm{NR}}(\omega)=2\,\mathrm{Re}[E^{(1)*}_{\mathrm{sc}}(\boldsymbol{R},\omega)E^{(3)}_{\mathrm{sc}}(\boldsymbol{R},\omega)]/E^2N^2$$
$$\propto-\mathrm{Re}\left(\sum_{\lambda'}G^*_{\lambda'}(\omega)\sum_{\lambda\mu}|G_{\lambda}(\omega)|^2\right.$$
$$\left.\times G^2_{\mu}(\omega)F^{-1}_{\lambda\mu}(0,2\omega)\right)\Big/N^2\,, \quad (23)$$

where

$$G_\lambda(\omega) \equiv \sum_\mu G_{\lambda\mu}(k_x=0,\omega)$$

$$= \sum_\mu G_{\mu\lambda}(k_x=0,\omega)\,. \qquad (24)$$

We have set k_x, k_y, k'_x, k'_y to be zero since they are much smaller than the size of the Brillouin zone $1/a$.

We now consider the FWM experiment. Setting k_{ix}, $k_{iy}=0$, $i=1, 2, 3, 4$, we obtain $\gamma^{(3)}=\gamma^{(3)}[\hat{\boldsymbol{\mu}}-\hat{\boldsymbol{R}}(\hat{\boldsymbol{R}}\cdot\hat{\boldsymbol{\mu}})]\hat{\mu}\hat{\mu}\hat{\mu}\hat{\mu}$, and

$$\gamma^{(3)}(-\omega;\omega,-\omega,\omega) \propto \sum_{\lambda\mu} |G_\lambda(\omega)|^2 G_\mu^2(\omega)$$

$$\times F_{\lambda\mu}^{-1}(0,2\omega)/N\,. \qquad (25)$$

In all numerical calculations, we have set $\eta=1$ meV. Fig. 1a displays $S_{\rm LR}(\omega)$ (dashed line) and the single-photon resonance of $-S_{\rm NR}(\omega)$ (solid line) calculated for $J=10$ meV, $J'=100$ meV, $N=4$. The two positive resonances in $S_{\rm LR}(\omega)$ coincide with the two negative resonances in $S_{\rm NR}(\omega)$. In general for N wires, there are $\frac{1}{2}N^*$ positive resonances in $S_{\rm LR}(\omega)$ which coincide with the $\frac{1}{2}N^*$ single-photon resonance of $S_{\rm NR}(\omega)$, where $N^*=N$ for even N and $N^*=N+1$ for odd N. This reflects exciton confinement and inversion symmetry in the y direction [11]. The resonance frequencies are equal to the single exciton energies $\epsilon_\alpha(k_x=0)$, $\alpha=1, 3, \ldots, N^*-1$. States with even α are antisymmetric in the y direction, carry no oscillator strength, and do not contribute to the signal [10,11].

In addition to the two negative single-photon resonances shown in Fig. 1a, $S_{\rm NR}(\omega)$ have three dispersive features related to two-photon resonances, shown in Fig. 1b by solid lines. They coincide with the three discrete positive resonances of $\mathrm{Im}\,\gamma^{(3)}(\omega;\omega,-\omega,\omega)$, which are shown by dashed lines. These resonances come from the two-exciton states with zero center of mass momentum in the x direction.

When N is small (quasi 1D), single-photon resonances show up as negative peaks in $S_{\rm NR}(\omega)$ (see Fig. 1a, solid line), while two-photon resonances give dispersive features (see Fig. 1b, solid line). For large N, the single-photon resonances of $S_{\rm NR}(\omega)$ become dispersive as well. $S_{\rm NR}$ is dispersive since it contains both the linear and the third-order scattered field. On the other hand, $\gamma^{(3)}$ contains only $\boldsymbol{E}_{\rm sc}^{(3)}$ and has absorptive resonances. Numerical results for $S_{\rm NR}(\omega)$ near the single-photon resonance $\omega=\epsilon_1(k_x=0)$ and various values of N are displayed in Fig. 2. The figure shows how the lineshape evolves from negative absorptive resonance at 1D to a dispersive feature at

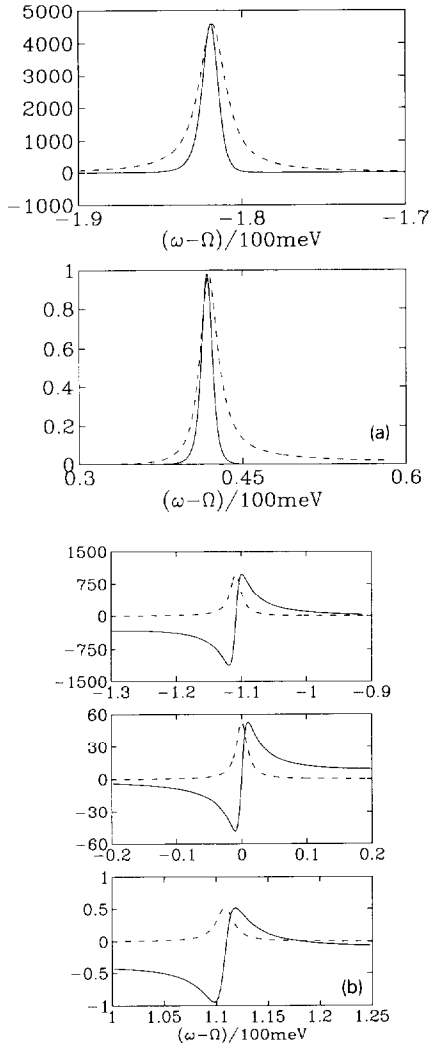

Fig. 1. (a) The linear scattering coefficient $S_{\rm LR}(\omega)$ (dashed line) and single-photon resonance of the nonlinear scattering coefficient $-S_{\rm NR}(\omega)$ (solid line) for a multiwire system with $N=4$, $J=10$ meV, $J'=100$ meV. The vertical scale shows the relative magnitude of $-S_{\rm NR}$. $S_{\rm LR}$ is normalized to have the same height as $-S_{\rm NR}$. The ratio of $S_{\rm LR}$ peaks in the upper and lower panels is 318:1. (b) The two-photon resonance of $S_{\rm NR}(\omega)$ (solid line) and $\mathrm{Im}\,\gamma^{(3)}(\omega;\omega,-\omega,\omega)$ (dashed line). The vertical scale shows the relative magnitude of $S_{\rm NR}$. The unit is smaller than that of (a) by about six orders of magnitude. $\mathrm{Im}\,\gamma^{(3)}$ is normalized to the same height as $S_{\rm NR}$. The ratio of $\mathrm{Im}\,\gamma^{(3)}$ peaks in the upper, middle and lower panels is 442:71:1.

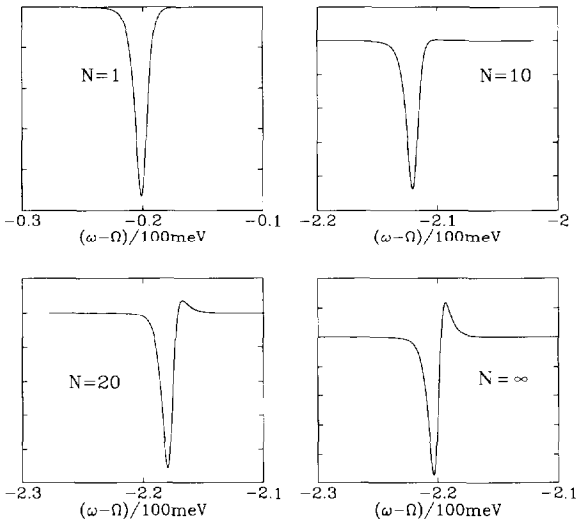

Fig. 2. The nonlinear scattering coefficient $S_{NR}(\omega)$ near the single-photon resonance $\omega=\epsilon_1(k_x=0)$ for a multiwire system with $J=10$ meV, $J'=100$ meV and various values N. $N=\infty$ corresponds to a two-dimensional lattice (quantum well).

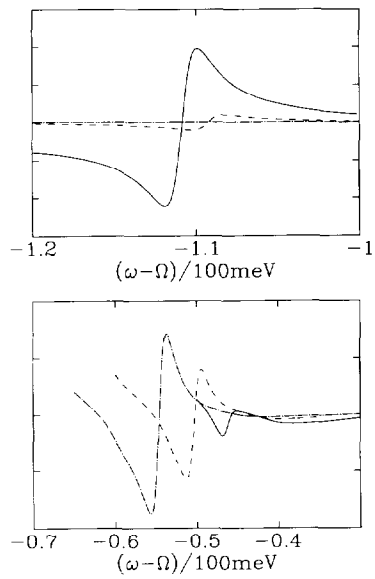

Fig. 3. The lowest frequency two-photon resonance of $S_{NR}(\omega)$ for a multiwire system with $N=4$ (solid line in the upper panel of Fig. 1b. In the upper panel, $J'=100$ meV is fixed, $J=10$ meV (solid line), 20 meV (dashed line), 30 meV (dash-dotted line). In the lower panel, $J=10$ meV is fixed, $J'=42$ meV (solid line), 46 meV (dashed line), 50 meV (dash-dotted line).

2D.

The lowest frequency two-photon resonance of $S_{NR}(\omega)$ (solid line in upper panel of Fig. 1b) for various values of J and J' is displayed in Fig. 3. The upper panel shows that the two-photon resonance decreases with J and at $J=30$ meV it disappears. The lower panel shows how the two-photon resonance increases with J'. This can be explained as follows: due to translational invariance in the x direction, the states contributing to the signal are single-exciton states with $k_x=0$, which are discrete, and two-exciton states whose center of mass momentum in the x direction is zero, but with arbitrary relative momentum. These states form several distinct bands with bandwidth proportional to J (see Eq. (16)). As J increases, the two-exciton bandwidth increases and the two-photon resonances vanish when neighboring two-exciton bands merge. On the other hand, the gap between neighbouring two-exciton bands is proportional to the interaction in the y direction J', and as J' increase, the two-photon resonance is enhanced.

We next study the dependence of the signal on the number of wires. We denote the peak magnitude of the lowest frequency single-photon resonance of $|S_{NR}(\omega)|$ (solid line in the upper panel of Fig. 1a) by A_N. Note that $A_N=|S_{NR}(\omega_m)|$, with ω_m close but not equal to $\epsilon_1(k_x=0)$. For interacting wires ($J'=0$), A_N is independent of N. For interacting wires, A_N is calculated numerically and is shown in Fig. 4. The figure illustrates how A_N increases linearly with N for

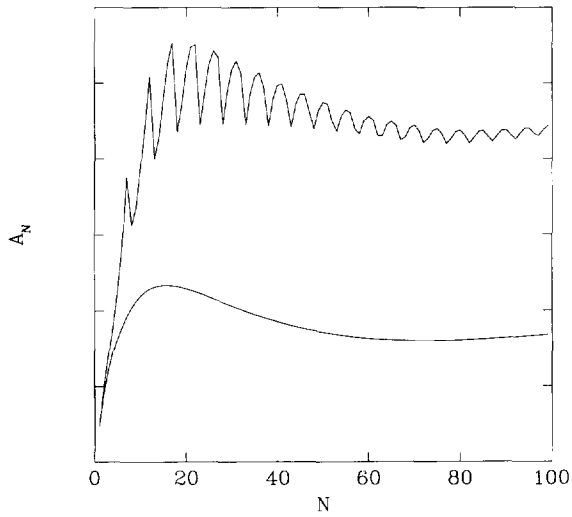

Fig. 4. A_N as a function of N. $J'=100$ meV. From bottom to top, $J=10$, -10 meV.

small N, and becomes independent of N for large N. This behavior has been discussed earlier [15,17,19]. The figure further shows that A_N first reaches a maximum, then attains a local minimum, and finally saturates. The interesting point is that when J and J' have opposite signs, A_N shows an oscillatory dependence on N.

We next define a coherence number N_c as the value of N which maximizes A_N. This reflects the number of chains which maximizes the cooperative nonlinear response. N_c as a function of J' for various values of J is displayed in Fig. 5a. The figure shows that N_c increases with increasing J' and decreasing J. When J is zero, there are N discrete single-exciton states. It was shown in Ref. [19] that for a regular molecular lattice with periodic boundary conditions, and when ω is on resonance with a single-exciton eigenstate, $\bar{\Gamma}$ increases linearly with the number of molecules, provided the lattice size is small so that the eigenstates are well separated. $\bar{\Gamma}$ becomes independent of the number of molecules when the lattice size is so large that neighboring eigenstates overlap. The crossover size is determined by the condition that the separation between eigenstates is equal to the linewidth. In our case, this implies $|\epsilon_1(0)-\epsilon_2(0)| \approx \eta$, which gives $N_c \sim \sqrt{J'/\eta}$. As J is turned on, each eigenstate develops into a band with bandwidth $4|J|$, and the energy width changes to $\eta+4|J|$. Therefore N_c is given approximately $\sqrt{J'/(4|J|+\eta)}$. This explains why N_c increases with J' and decreases with J.

In Fig. 5b, we show how A_{30} increase with J' for various values of J. Again we observe an oscillatory dependence of A_{30} on J' when J and J' have opposite signs. This can be explained as follows: the single-photon resonance intensity increases with $|E_2-2E_1|$, where E_2 and E_1 are the energies of two-exciton and single-exciton eigenstates [15]. In the following discussion we assume that the two-exciton eigenstates are direct products of single-exciton states, and the two-exciton energy is equal to the sum of single-exciton energies. This is not strictly true due to the hard core exclusion of excitons, nevertheless it allows us to qualitatively explain the results. The single-exciton state of interest is $|\alpha=1,\ k_x=0\rangle$, with energy $E_1=\epsilon_1(k_x=0)=-2J-2J'\cos[\pi/(N+1)]$. The two-exciton states contributing to the signal are $|\alpha,k'_x\rangle\otimes|\beta,-k'_x\rangle$ (note that the center of mass momentum is zero), with

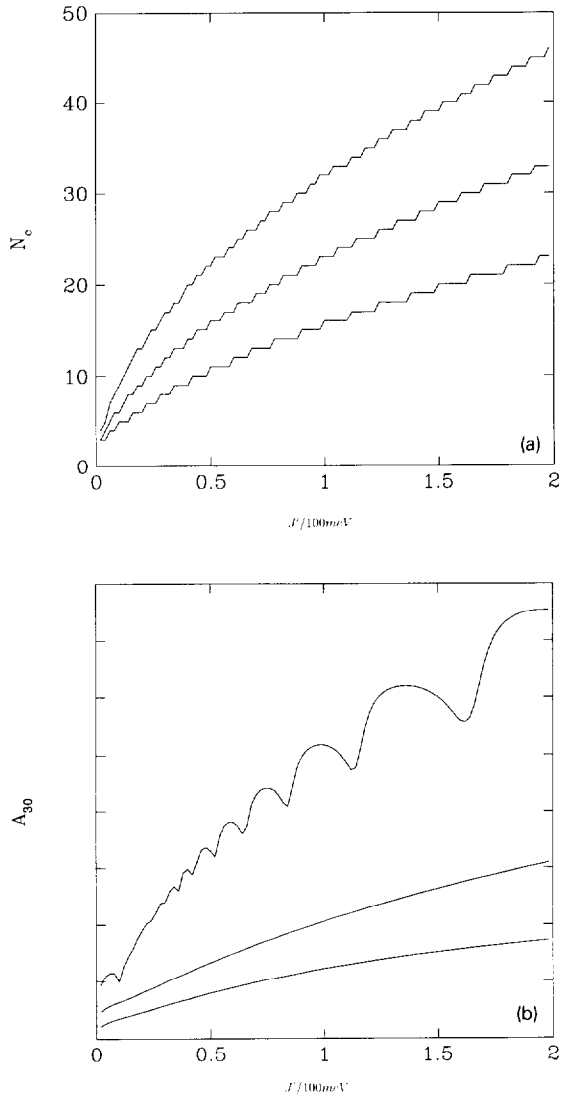

Fig. 5. (a) The coherence size N_c as a function of J'. From top to bottom $J=0$, 1, 10 meV. (b) A_{30} (30 wires) as a function of J'. $J=1$, 10, -10 meV from bottom to top.

$$E_2=\epsilon_\alpha(k'_x)+\epsilon_\beta(-k'_x)=-4J\cos(k'_x a) -2J'\cos[\alpha\pi/(N+1)]-2J'\cos[\beta\pi/(N+1)]\,.$$

Therefore

$$E_2-2E_1=4J(1-\cos k'_x a)+2J'\{2\cos[\pi/(N+1)] -\cos[\alpha\pi/(N+1)]-\cos[\beta\pi/(N+1)]\}\,. \quad (26)$$

If $J, J' > 0$, $|E_2 - 2E_1|$ increases with J'. This is why A_{30} grows with J'. If $J < 0$ and $J' > 0$, for some k'_x values $|E_2 - 2E_1|$ increases with J', while for other k'_x values $|E_2 - 2E_1|$ decreases with J'. Therefore as J' increases, some two-exciton energies move closer to twice the single-exciton energy, and thus reduce the single-photon resonance peak, while others move away from $2E_1$ and increase this peak. This is why A_{30} is no longer a monotonic function of J', and shows an oscillatory behavior (see Fig. 5b).

In summary, we have calculated the linear and the nonlinear scattering signal from an assembly of N interacting quantum wires. For small N, the single-photon resonance of $S_{NR}(\omega)$ is negative and absorptive reflecting the saturation of the single-exciton transition, whereas the two-photon resonances of $S_{NR}(\omega)$ are dispersive. For large N, the single-photon resonances become dispersive as well. The two-photon resonances and the coherence size increase with interwire interaction J' and decrease with intrawire J interaction. When J and J' have opposite signs the nonlinear signal shows oscillatory dependence on N and J'.

Finally in the present work we considered perfect periodic nanostructures. Effects of disorder in geometry, defects, as well as coupling to nuclear motions require a proper averaging of the product of Green functions and may result in additional interesting resonances. These can be carried out using diagrammatic or semiclassical techniques [14,21].

The support of the National Science Foundation and the Air Force Office of Scientific Research is gratefully acknowledged. We wish to thank Dr. Vladimir Chernyak for most useful discussions.

References

[1] H. Fidder, J. Knoester and D.A. Wiersma, J. Chem. Phys. 98 (1993) 6564.
[2] A.E. Johnson, S. Kumazaki and K. Yoshihara, Chem. Phys. Letters 211 (1993) 511.
[3] F.F. So and S.R. Forrest, Phys. Rev. Letters 66 (1991) 2649.
[4] M. Pope and C.E. Swenberg, Electronic processes in organic crystals (Oxford Univ. Press, Oxford, 1982).
[5] J. Knoester and S. Mukamel, Phys. Rept. 205 (1991) 1; O. Dubovsky and S. Mukamel, J. Chem. Phys. 96 (1992) 9201.
[6] J. Bounds and W. Siebrand, Chem. Phys. Letters 75 (1980) 414.
[7] E.A. Silinsh, Organic molecular crystals (Springer, Berlin, 1980).
[8] M. Orrit and Ph. Kottis, Advan. Chem. Phys. 74 (1988) 1.
[9] K. Minoshima, M. Taiji, K. Misawa and T. Kobayashi, Chem. Phys. Letters 218 (1994) 67.
[10] Z.K. Tang, A. Yanase, T. Yasui, Y. Segawa and K. Cho, Phys. Rev. Letters 30 (1993) 1431.
[11] N. Wang, J.K. Jenkins, V. Chernyak and S. Mukamel, Phys. Rev. B 49 (1994) 17079.
[12] D. Mobius and H. Kuhn, Israel J. Chem. 18 (1979) 375; J. Appl. Phys. 64 (1988) 5138.
[13] J. Knoester, Phys. Rev. Letters 68 (1992) 654.
[14] N. Wang, A.A. Muenter and S. Mukamel, J. Chem. Phys. 99 (1993) 3604;
N. Wang, V. Chernyak and S. Mukamel, Phys. Rev. B, to be published.
[15] F.C. Spano and S. Mukamel, Phys. Rev. Letters 66 (1991) 1197.
[16] D.S. Chemla and J. Zyss, Nonlinear optical properties of organic molecules and crystals, Vols. I, II (Academic Press, New York, 1987).
[17] H. Ishihara and K. Cho, Mol. Cryst. Liquid Cryst. Sci. Technol. B 4 (1993) 81; Intern. J. Nonlin. Opt. Phys. 1 (1992) 287.
[18] V. Chernyak and S. Mukamel, J. Chem. Phys. 100 (1994) 2953; Phys. Rev. B 48 (1993) 2470.
[19] N. Wang, V. Chernyak and S. Mukamel, J. Chem. Phys. 100 (1994) 2465.
[20] E.N. Economou, Green functions in quantum physics (Springer, Berlin, 1983).
[21] N. Wang, J.A. Leegwater and S. Mukamel, J. Chem. Phys. 98 (1993) 5899;
J.A. Leegwater and S. Mukamel, J. Chem. Phys., in press.